

# MANGO: A GLOBAL SINGLE-DATE PAIRED DATASET FOR MANGROVE SEGMENTATION

Junhyuk Heo, Beomkyu Choi, Hyunjin Shin, Darongsae Kwon

TelePIX

07330, Seoul, South Korea

{jhj1037, bkchoi, hyunjin, darong.kwon}@telepix.net

**Abstract**—Mangroves are critical for climate-change mitigation, requiring reliable monitoring for effective conservation. While deep learning has emerged as a powerful tool for mangrove detection, its progress is hindered by the limitations of existing datasets. In particular, many resources provide only annual map products without curated single-date image-mask pairs, limited to specific regions rather than global coverage, or remain inaccessible to the public. To address these challenges, we introduce MANGO, a large-scale global dataset comprising 42,703 labeled image-mask pairs across 124 countries. To construct this dataset, we retrieve all available Sentinel-2 imagery within the year 2020 for mangrove regions and select the best single-date observations that align with the mangrove annual mask. This selection is performed using a target detection-driven approach that leverages pixel-wise coordinate references to ensure adaptive and representative image-mask pairings. We also provide a benchmark across diverse semantic segmentation architectures under a country-disjoint split, establishing a foundation for scalable and reliable global mangrove monitoring. The datasets and code is available at <https://github.com/ROKMC1250/MANGO>.

**Index Terms**—Mangroves, Remote Sensing, Deep Learning, Semantic Segmentation, Dataset, Sentinel-2

## I. INTRODUCTION

Mangrove forests are a critical “blue carbon” ecosystem, storing large amounts of carbon in both biomass and soils while providing shoreline protection and habitat support [1, 2]. Despite occupying a relatively small coastal footprint, their loss translates into outsized impacts on carbon budgets and coastal resilience [1, 2].

Remote sensing has become the primary modality for large-scale monitoring, with many operational pipelines relying on spectral analysis, such as the Normalized Difference Vegetation Index (NDVI) and Mangrove Vegetation Index (MVI), followed by thresholding [3, 2]. While these approaches are attractive due to their simplicity, they suffer from two structural limitations: (i) decision rules require explicit thresholds sensitive to acquisition conditions, and (ii) these thresholds rarely transfer across diverse coastlines due to spectral confounders like sediment and mixed pixels [3, 4]. These limitations are evident in Fig. 1, where two Sentinel-2 Level-2A (S2 L2A) acquisitions over the same site appear visually similar but yield markedly different MVI responses, making threshold-based rules unstable.

Recent studies have increasingly leveraged deep learning for mangrove segmentation, achieving higher accuracy than traditional spectral indices [5–8]. However, the advancement

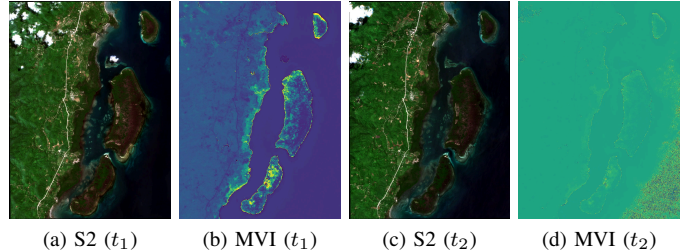


Fig. 1. Spectral-index instability. MVI responses for the same site at different dates ( $t_1, t_2$ ) show significant drift despite visual similarities in RGB composites.

of these models is significantly constrained by data-related bottlenecks. First, existing mangrove datasets are often geographically limited to specific regions [5, 9] or rely on temporally aggregated median composites that result in blurry, synthetic representations of forests [8, 10]. More importantly, global products such as Global Mangrove Watch (GMW) [11] and High-resolution Global Mangrove Forests (HGMF) [12] lack curated, single-date Sentinel-2 pairings, which are essential for real-time monitoring. We define this lack of curated image-label pairs as the “temporal pairing gap,” a major barrier preventing global benchmarking and scalable deployment.

To bridge this gap, we introduce MANGO, a large-scale global dataset comprising 42,703 curated image-mask pairs across 124 countries. MANGO is constructed through a two-stage pipeline: data collection via Google Earth Engine [14], followed by an adaptive selection process using a target detection-driven approach to identify the most representative single-date imagery for each site. Furthermore, we establish a standardized benchmark evaluated under a country-disjoint split protocol to ensure geographic generalization across diverse coastal contexts. We evaluate various architectures, including CNN-based models [15–17] and Transformer-based models [18–21], to demonstrate the impact of our quality-driven selection strategy. The primary contributions are as follows:

- **MANGO Dataset:** A global, large-scale mangrove segmentation dataset with 42,703 paired Sentinel-2 L2A images and GMW labels.
- **Temporal Pairing Gap:** We resolve the temporal pairing

TABLE I

COMPARISON OF MANGO WITH EXISTING PRODUCTS AND DATASETS. AVAILABILITY REFERS TO THE ACTUAL PUBLIC ACCESSIBILITY OF RAW IMAGE-LABEL PAIRS; NOTABLY, REPOSITORIES MARKED WITH  $\dagger$  ARE NOT PRACTICALLY ACCESSIBLE DESPITE BEING MENTIONED AS AVAILABLE IN THEIR ORIGINAL PAPERS.

Dataset	Scope	Res. (m)	Sensor	1:1 Pair	Samples	Patch Size	Split Strategy	Availability
GMW v3.0 [11]	Global	25	SAR / Landsat	No	N/A	N/A	N/A	Map Only
HGMF_2020 [12]	Global	10	Sentinel-2	No	N/A	N/A	N/A	Map Only
ME-Net [5]	Regional	10	Sentinel-2	Yes	5,120	256 $\times$ 256	Random	Restricted
TCCFNet [9]	Regional	0.3	VHR	Yes	1,024	768 $\times$ 768	Random	Restricted
MagSet-2 [13]	Global	10	Sentinel-2	Yes	10,000+	128 $\times$ 128	Random	Restricted $\dagger$
MANGO (Ours)	Global	10	Sentinel-2	Yes	42,703	256 $\times$ 256	Country-disjoint	Public

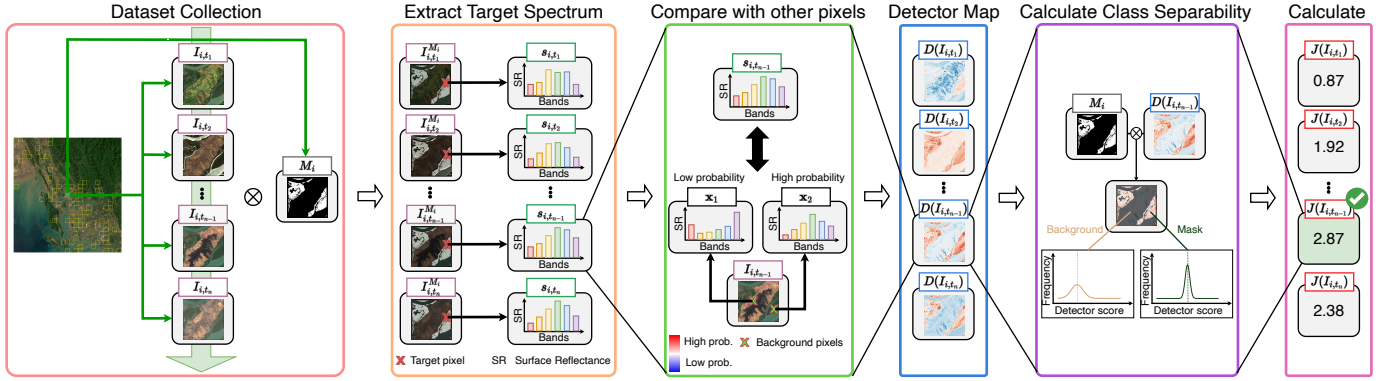


Fig. 2. Scene selection pipeline for constructing single-date image-mask pairs from annual mangrove labels. For each site, multiple Sentinel-2 candidates  $\{I_{i,t}\}$  share the same annual mask  $M_i$ . We extract mangrove reference pixels from  $M_i$  to form a target spectrum and compute a detection map  $D_{i,t}$  using a background-whitened target detector. Each candidate is scored by the Fisher discriminant ratio  $J(I_{i,t})$  over mangrove and background regions, and the final acquisition is selected by  $t^* = \arg \max_t J(I_{i,t})$ .

gap by selecting, for each scene, the Sentinel-2 L2A image that best matches the GMW label using scene-adaptive target detector.

- **Benchmark:** We benchmark diverse segmentation backbones under a country-disjoint split for global generalization.

## II. RELATED WORK

Mangrove monitoring traditionally relies on multispectral indices like MVI and NDVI [22, 23, 3], which often require site-specific retuning due to coastal heterogeneity and spectral confounders like sediment and mixed pixels [4, 3]. While deep learning models offer a robust alternative [24, 18], their progress is constrained by the availability of curated global training data [25, 11, 12]. As shown in Table I, existing products such as GMW [11] and HGMF [12] provide extensive maps but lack the 1:1 image-mask pairings required for supervised training. Meanwhile, regional datasets like ME-Net [5] and TCCFNet [9] are limited by small sample sizes and frequently restricted public accessibility. MagSet-2 [13] offers more samples but uses March–June composite Sentinel-2 imagery rather than selecting a single-date scene, and utilizes simple random split strategies. In contrast, MANGO establishes a public, large-scale benchmark of single-date 1:1 pairings across 124 countries, employing a country-disjoint split to ensure rigorous geographic generalization.

## III. CONSTRUCTING MANGO

The construction of MANGO is a multi-stage process designed to resolve the temporal pairing gap by identifying the best match between annual labels and single-date observations. As illustrated in Fig. 2, the pipeline consists of scalable data collection via GEE [14] followed by an adaptive selection process. This ensures that each sample in the dataset is the most representative scene for its geographic site.

### A. Dataset Collection

We tile the GMW [11] extent into a set of regions  $\mathcal{R} = \{R_i\}$ , where each  $R_i$  is a  $256 \times 256$  pixel patch at 10 m resolution [11]. For each sensing date  $t$ , we denote the corresponding Sentinel-2 L2A acquisition over  $R_i$  by  $I_{i,t} \in \mathbb{R}^{256 \times 256 \times 13}$ . For each  $R_i$ , we define the candidate pool  $\mathcal{I}_i$  of S2 L2A [26] acquisitions  $I_{i,t}$  as follows:

$$\mathcal{I}_i = \{I_{i,t} \mid t \in \mathcal{T}_i, C(I_{i,t}) < \kappa, \Omega(I_{i,t}) \geq \omega\}, \quad (1)$$

where  $\mathcal{T}_i$  denotes the sensing dates within the target year 2020 [11]. To ensure data quality, we define  $C(I_{i,t})$  as the cloud fraction calculated using the cloud mask provided by GEE [14], and  $\Omega(I_{i,t})$  as the spatial coverage of the area of interest within the region. We set the strict filtering thresholds to  $\kappa = 0.05$  and  $\omega = 0.50$ . In total, this pipeline retrieved 1,379,743 images across 42,703 regions, providing an average of 32 candidates per site for the subsequent selection stage.

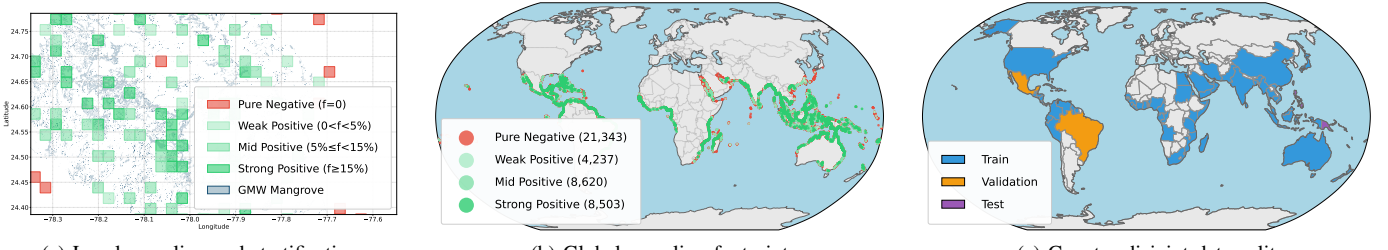


Fig. 3. Global overview and experimental setup of the MANGO dataset. (a) illustrates the categorization of tiles into positive and negative classes. (b) shows the distribution of MANGO images across diverse countries. (c) visualizes the geographic partition used for rigorous generalization testing.

The collection is categorized by the mangrove fraction  $f_i = M_{GMW} \cap R_i / R_i$  into four levels: (i) strong positive ( $f_i \geq 0.15$ ), (ii) mid positive ( $0.05 \leq f_i < 0.15$ ), (iii) weak positive ( $0 < f_i < 0.05$ ), and (iv) pure negative ( $f_i = 0$ ). We enforce a 1:1 ratio between total positive and negative samples to mitigate class imbalance, a common challenge in binary segmentation [27, 28]. Furthermore, the positive subset follows a 2:2:1 ratio for strong, mid, and weak classes, respectively. This ensures sufficient representation of fragmented coastal fringes and low-density stands, which are often underrepresented in global maps [29].

#### B. Dataset Selection

The selection stage identifies the optimal acquisition  $I_{i,t^*} \in \mathcal{I}_i$  by finding the best match between single-date Sentinel-2 observations and annual GMW masks. For each region  $R_i$ , we select the sensing date  $t^*$  that provides the most distinct separability between mangroves and the coastal background. **Target Detection Phase:** To obtain a representative target signature, we apply binary erosion to the annual mask  $M_i$  using a  $5 \times 5$  structural element, identifying  $K = 10$  high-purity coordinates  $\mathcal{P} = \{\mathbf{p}_k\}_{k=1}^K$ , where  $I_{i,t}(\mathbf{p}) \in \mathbb{R}^{13}$  denotes the spectral vector at pixel location  $\mathbf{p}$ . The target spectrum  $\mathbf{s}_{i,t}$  is calculated as:

$$\mathbf{s}_{i,t} = \frac{1}{|\mathcal{P}|} \sum_{\mathbf{p} \in \mathcal{P}} I_{i,t}(\mathbf{p}). \quad (2)$$

For each candidate image  $I_{i,t}$ , we apply a matched filter detector [30] to generate a continuous detection map  $D_{i,t}$ . We first estimate the background mean  $\mu_{i,t}$  and covariance  $\Gamma_{i,t}$  from background pixels, and compute a background-normalized match score for each pixel  $\mathbf{x}$ :

$$D_{i,t}(\mathbf{x}) = \frac{\mathbf{s}_{i,t}^\top \Gamma_{i,t}^{-1} (\mathbf{x} - \mu_{i,t})}{\sqrt{\mathbf{s}_{i,t}^\top \Gamma_{i,t}^{-1} \mathbf{s}_{i,t}}}. \quad (3)$$

The resulting map  $D_{i,t}$  represents a covariance-normalized target match score, suppressing background variability through whitening.

**Evaluation and Ranking Phase:** To quantify the quality of each candidate, we define two disjoint pixel sets based on the annual mask  $M_i$ : the mangrove set  $\Omega_{m,i} = \{\mathbf{x} \in R_i | M_i(\mathbf{x}) = 1\}$  and the background set  $\Omega_{b,i} = \{\mathbf{x} \in R_i | M_i(\mathbf{x}) = 0\}$ . The

class-wise mean and variance are calculated from the detection scores as follows:

$$\mu_{c,t} = \text{mean}(D_{i,t}(\Omega_{c,i})), \quad \sigma_{c,t}^2 = \text{var}(D_{i,t}(\Omega_{c,i})), \quad (4)$$

where  $c \in \{m, b\}$  denotes the class index. We then evaluate the class separability using the Fisher discriminant ratio (FDR),  $J(I_{i,t})$ :

$$J(I_{i,t}) = \frac{(\mu_{m,t} - \mu_{b,t})^2}{\sigma_{m,t}^2 + \sigma_{b,t}^2}. \quad (5)$$

The optimal acquisition  $t^*$  for region  $i$  is determined by finding the date that maximizes this separability criterion:

$$t^* = \arg \max_{t \in \mathcal{T}_i} J(I_{i,t}). \quad (6)$$

**Spectral Index Comparison:** For comparative analysis, we also evaluate a selection strategy based on the MVI [22]. In this case, the MVI response map is substituted for the detection map  $D_{i,t}$ , and the same FDR-based ranking is applied. This framework ensures that the most representative observation is selected across diverse coastal environments, providing a standardized baseline for the deep learning models evaluated in the following section IV-B.

#### C. Dataset Information

The MANGO dataset consists of 42,703 curated 13-band image-mask pairs at 10 m resolution, spanning 124 countries. As shown in Fig. 3b, these samples are distributed worldwide to capture diverse coastal environments, with a composition of 21,424 Pure Negative, 4,258 Weak Positive, 8,643 Mid Positive, and 8,517 Strong Positive images. These categories are defined based on the mangrove fraction within each tile relative to the GMW annual label as illustrated in Fig. 3a. To ensure a robust evaluation of geographic generalization, we adopt a country-disjoint split protocol with an 8:1:1 ratio for training, validation, and testing (Fig. 3c). By evaluating models on entirely unseen geographic regions, this strategy effectively prevents performance overestimation due to spatial autocorrelation and ensures that the learned features are applicable across varied global coastal contexts.

TABLE II

BENCHMARK RESULTS OF SEGMENTATION MODELS ON THE MANGO COUNTRY-DISJOINT TEST SET, COMPARING DATASETS CONSTRUCTED VIA MVI-BASED [22] AND MF-BASED [30] SELECTION PROTOCOLS. FORMATTING: **BOLD** MARKS THE BEST SCORE IN EACH COLUMN AND UNDERLINE MARKS THE SECOND BEST.

Selection	Metric	UNet++ [15]	MANet [16]	PAN [17]	SegFormer [18]	FPN [19]	DPT [20]	UPerNet [21]
MVI-based [22]	IoU (%)	87.73	87.93	88.92	89.95	91.10	86.15	88.54
	F1 (%)	89.49	89.79	90.72	91.73	92.66	87.55	90.29
MF-based [30]	IoU (%)	<b>91.47</b>	<u>91.29</u>	90.30	87.56	90.70	84.84	88.73
	F1 (%)	<b>93.21</b>	<u>93.00</u>	92.05	89.50	92.48	86.88	90.66

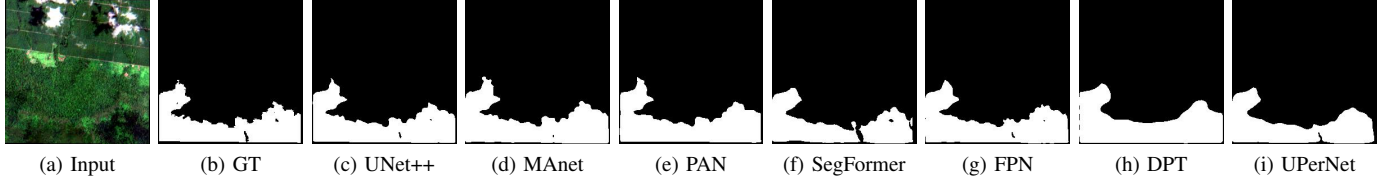


Fig. 4. Qualitative results across baseline models. (a) Sentinel-2 L2A imagery, (b) MANGO ground-truth mask established via the quality-aware selection pipeline, and (c-i) segmentation predictions from baseline models.

#### IV. EXPERIMENTS

All experiments were implemented in PyTorch using NVIDIA RTX 4090 GPUs. Models were optimized via AdamW with  $10^{-3}$  learning rate for 50 epochs under identical hyperparameter configurations to ensure a consistent comparison. We evaluate standard semantic segmentation metrics and conduct all evaluations on the MANGO country-disjoint split.

##### A. Benchmark Results

We report two complementary outcomes: (i) benchmark performance across seven segmentation architectures on the MANGO country-disjoint test set, and (ii) selection results comparing datasets constructed via MVI-based [22] and MF-based [30] selection. As shown in Table II, MF-based selection improves performance over the MVI-based baseline across models, with UNet++ [15] achieving the best IoU and F1, and MANet [16] being the second best. Figure 4 provides qualitative evidence that the MF-based selection yields clear supervision under diverse coastal conditions, supporting robust global generalization under the country-disjoint split.

##### B. Selection Visualization

Figure 5 illustrates two candidates from the same region acquired at different times. Under MVI-based selection, the FDR score  $J(I_{i,t})$  is often markedly lower, indicating limited separability between mangrove and background. This behavior is consistent with the use of a fixed spectral-index formulation, which can be confounded by coastal spectral variability and leads to visible false positives in sediment-rich water and mixed pixels. In contrast, MF-based selection yields higher  $J(I_{i,t})$  scores and cleaner response maps by adapting the target matching to each scene, thereby reducing background-induced errors and improving mangrove–background discrimination for reliable single-date pairing.

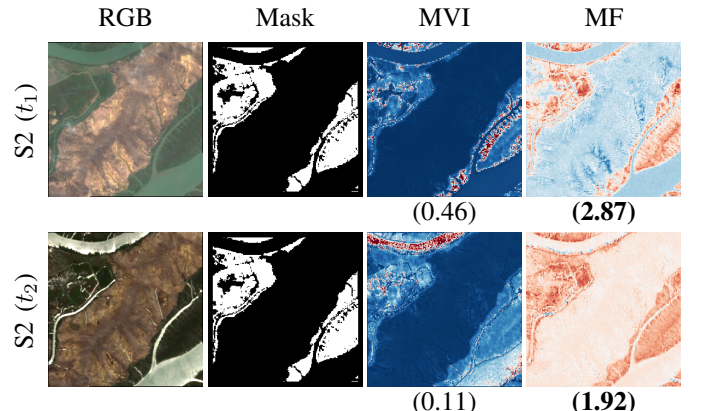


Fig. 5. Selection comparison for two Sentinel-2 candidate observations ( $t_1$  and  $t_2$ ) from the same region. The mask is the shared GMW-derived annual label. MVI and MF maps show per-pixel responses, and the values in parentheses report the FDR score  $J(I_{i,t})$  used to rank candidates.

#### V. CONCLUSION

We presented MANGO, a public global dataset of 42,703 single-date Sentinel-2 image-mask pairs spanning 124 countries, designed to enable supervised mangrove segmentation at scale. To bridge the temporal pairing gap between annual labels and single-date observations, we select for each site the most representative acquisition by scoring target-detector responses with class separability. Benchmarking under a country-disjoint split shows that MF-based selection improves segmentation performance over the spectral-index baseline, providing cleaner supervision across diverse coastal conditions. We expect MANGO to support reproducible benchmarking and more reliable global mangrove monitoring for conservation and climate-related applications.

## REFERENCES

- [1] D. C. Donato, J. B. Kauffman, D. Murdiyarso, S. Kurnianto, M. Stidham, and M. Kanninen, “Mangroves among the most carbon-rich forests in the tropics,” *Nature Geoscience*, vol. 4, pp. 293–297, 2011.
- [2] D. Wang and M. Jia, “A review of remote sensing for mangrove forests: 1956–2018,” *Remote Sensing of Environment*, vol. 231, p. 111223, 2019.
- [3] D. Tran *et al.*, “A review of spectral indices for mangrove remote sensing,” *Remote Sensing*, vol. 14, no. 19, p. 4868, 2022.
- [4] M. P. Neri, A. B. Baloloy, and A. C. Blanco, “Limitation assessment and workflow refinement of the mangrove vegetation index (mvi)-based mapping methodology using sentinel-2 imagery,” in *The International Archives of the Photogrammetry, Remote Sensing and Spatial Information Sciences*, vol. XLVI-4/W6-2021, 2021, pp. 235–242.
- [5] M. Guo *et al.*, “ME-Net: A deep convolutional neural network for extracting mangrove using sentinel-2a data,” *Remote Sensing*, 2021.
- [6] H. Dong *et al.*, “Mangroveseg: Deep-supervision-guided feature aggregation network for mangrove detection and segmentation in satellite images,” *Forests*, 2024.
- [7] Y. Zhang *et al.*, “MW-SAM: Mangrove wetland remote sensing image segmentation network based on segment anything model,” *IET Image Processing*, 2024.
- [8] R. Kathiroli *et al.*, “Spatiotemporal analysis of mangroves using median composites and convolutional neural network,” *Scientific Reports*, 2025.
- [9] L. Fu, Y. Wang *et al.*, “Tccfnet: a semantic segmentation method for mangrove remote sensing images based on two-channel cross-fusion networks,” *Frontiers in Marine Science*, vol. 12, p. 1535917, 2025.
- [10] D. Hicks, R. Kastner, C. Schurgers, A. Hsu, and O. Aburto, “Mangrove ecosystem detection using mixed-resolution imagery with a hybrid-convolutional neural network,” in *NeurIPS 2020 Workshop on Tackling Climate Change with Machine Learning*, 2020. [Online]. Available: <https://www.climatechange.ai/papers/neurips2020/23>
- [11] P. Bunting, A. Rosenqvist, L. Hilarides, R. M. Lucas, N. Thomas, T. Tadono, T. A. Worthington, M. Spalding, N. J. Murray, and L.-M. Rebelo, “Global mangrove extent change 1996–2020: Global mangrove watch version 3.0,” *Remote Sensing*, vol. 14, no. 15, p. 3657, 2022.
- [12] M. Jia *et al.*, “Mapping global distribution of mangrove forests at 10-m resolution,” *Science Bulletin*, 2023.
- [13] L. J. V. de Souza, I. V. R. Zreik, A. Salem-Sermanet, N. Seghouani, and L. Pourchier, “A deep learning-based approach for mangrove monitoring,” *arXiv preprint arXiv:2410.05443*, 2024.
- [14] N. Gorelick, M. Hancher, M. Dixon, S. Ilyushchenko, D. Thau, and R. Moore, “Google earth engine: Planetary-scale geospatial analysis for everyone,” *Remote Sensing of Environment*, vol. 202, pp. 18–27, 2017.
- [15] Z. Zhou, M. M. R. Siddiquee, N. Tajbakhsh, and J. Liang, “Unet++: A nested u-net architecture for medical image segmentation,” in *International workshop on deep learning in medical image analysis*, 2018, pp. 3–11.
- [16] T. Fan, G. Wang, Y. Li, and H. Wang, “Ma-net: A multi-scale attention network for liver and tumor segmentation,” *IEEE Access*, vol. 8, pp. 179 656–179 665, 2020.
- [17] H. Li, P. Xiong, J. An, and L. Wang, “Pyramid attention network for semantic segmentation,” *arXiv preprint arXiv:1805.10180*, 2018.
- [18] E. Xie, W. Wang, Z. Yu, A. Anandkumar, J. M. Alvarez, and P. Luo, “Segformer: Simple and efficient design for semantic segmentation with transformers,” *Advances in Neural Information Processing Systems (NeurIPS)*, vol. 34, pp. 12 077–12 090, 2021.
- [19] T.-Y. Lin, P. Dollár, R. Girshick, K. He, B. Hariharan, and S. Belongie, “Feature pyramid networks for object detection,” in *Proceedings of the IEEE conference on computer vision and pattern recognition*, 2017, pp. 2117–2125.
- [20] R. Ranftl, A. Bochkovskiy, and V. Koltun, “Vision transformers for dense prediction,” in *Proceedings of the IEEE/CVF international conference on computer vision*, 2021, pp. 12 179–12 188.
- [21] T. Xiao, Y. Liu, B. Zhou, Y. Jiang, and J. Sun, “Unified perceptual parsing for scene understanding,” in *Proceedings of the European conference on computer vision (ECCV)*, 2018, pp. 418–434.
- [22] A. B. Baloloy, A. C. Blanco, R. R. C. Sta. Ana, and K. Nadaoka, “Development and application of a new mangrove vegetation index (mvi) for rapid and accurate mangrove mapping,” *ISPRS Journal of Photogrammetry and Remote Sensing*, vol. 166, pp. 95–117, 2020.
- [23] J. W. Rouse, R. H. Haas, J. A. Schell, and D. W. Deering, “Monitoring vegetation systems in the great plains with ERTS,” in *Proceedings of the Third Earth Resources Technology Satellite-1 Symposium*, ser. NASA SP-351. NASA, 1974, pp. 309–317.
- [24] O. Ronneberger, P. Fischer, and T. Brox, “U-net: Convolutional networks for biomedical image segmentation,” *International Conference on Medical Image Computing and Computer-Assisted Intervention (MICCAI)*, pp. 234–241, 2015.
- [25] C. Giri, E. Ochieng, L. L. Tieszen, Z.-L. Zhu, A. Singh, T. R. Loveland, J. G. Masek, and N. Duke, “Status and distribution of mangrove forests of the world using earth observation satellite data,” *Global Ecology and Biogeography*, vol. 20, no. 1, pp. 154–159, 2011.
- [26] M. Drusch, U. Del Bello, S. Carlier, O. Colin, V. Fernandez, F. Gascon, B. Hoersch, C. Isola, P. Laberinti, P. Martimort *et al.*, “Sentinel-2: ESA’s optical high-resolution mission for GMES operational services,” *Remote Sensing of Environment*, vol. 120, pp. 25–36, 2012.
- [27] I. Demir, K. Koperski *et al.*, “Deepglobe 2018: A challenge to parse the earth through satellite images,” in *Proceedings of the IEEE Conference on Computer Vision and Pattern Recognition Workshops*, 2018, pp. 172–181.
- [28] D. Bonafilia, B. Tellman *et al.*, “Sen1floods11: A georeferenced dataset to train and test deep learning flood algorithms for sentinel-1,” in *Proceedings of the IEEE/CVF Conference on Computer Vision and Pattern Recognition Workshops*, 2020, pp. 210–211.
- [29] J. R. Cissell, S. W. J. Canty, M. K. Steinberg, and L. T. Simpson, “Mapping national mangrove cover for belize using google earth engine and sentinel-2 imagery,” *Applied Sciences*, vol. 11, no. 9, p. 4258, 2021.
- [30] D. R. Fuhrmann, E. J. Kelly, and R. Nitzberg, “A cfar adaptive matched filter detector,” *IEEE Trans. Aerosp. Electron. Syst.*, vol. 28, no. 1, pp. 208–216, 1992.